RSC Advances

ROYAL SOCIETY OF CHEMISTRY

www.rsc.org/advances

RSC Advances

ARTICLE

High transparent conducting cerium incorporated CdO thin films deposited by spray pyrolytic technique

Received 00th January 20xx,
Accepted 00th January 20xx

DOI: 10.1039/x0xx00000x

www.rsc.org/

P. Velusamy[1], R. Ramesh Babu[1,*], K. Ramamurthi[2], M. S. Dahlem[3], E. Elangovan[3]

In the present work, spray pyrolysis technique was employed to deposit cerium (Ce) doped cadmium oxide (CdO) thin films with low level doping concentrations (0.25, 0.50, 0.75 and 1.0 wt. %). The crystallite size and lattice parameter values were estimated from X-ray diffraction analysis. X-ray diffraction patterns reveal the shift of preferential growth orientation from (111) to (200) planes on incorporating Ce in CdO matrix. The oxidation state of Ce, Cd and O in the deposited films was determined by X-ray photoelectron spectroscopic (XPS) studies. Surface microstructures of the films were analyzed by atomic force microscopy and their surface nature was studied by field emission scanning electron microscopy (FE-SEM). Electrical properties of the deposited films were determined by Hall measurements in van der Pauw configuration. The charge carrier concentration of CdO thin film is increased from 1.0×10^{20} cm^{-3} to 3.85×10^{20} cm^{-3} on doping 0.50 wt. % Ce; whereas, resistivity is decreased from 9.32×10^{-4} Ω cm to 3.81×10^{-4} Ω cm. The deposited Ce- doped CdO thin films for various concentrations showed increase in the average optical transmittance to 85 % from that of 72% of CdO film in the visible and NIR region. The band gap was gradually increased from 2.38 eV to 2.63 eV due to increase in the Ce doping at various levels. The emission properties of CdO and Ce doped CdO thin films were studied by photoluminescence spectrum recorded at room temperature. Figure of merit estimated for 0.50 wt. % of Ce doped CdO film is 9.18×10^{-3} Ω^{-1}.

Introduction

Transparent conducting oxides (TCOs) such as pure and doped cadmium oxide (CdO), zinc oxide (ZnO), tin oxide (SnO_2), and indium oxide (In_2O_3) play an important role in optoelectronic device application due to their unique combination of high electrical conductivity and high visible-NIR optical transmittance. Among the available TCOs, CdO has been considered as a promising material for solar cell, optical communication, phototransistor and IR heat mirror applications [1-3]. In particular, CdO thin films can be used as window layers instead of cadmium sulfide in cadmium sulfide (n-CdS)/cadmium telluride (p-CdTe) hetero-structured solar cells [4, 5]. Non-stoichiometric CdO possesses n- type semiconducting behavior due to the donor state of Cd interstitial or oxygen vacancies and it gives rise to a well-defined impurity band, which grows and merges with the conduction band [6]. Non-stoichiometric CdO thin films have low resistivity (ranging 10^{-2} to 10^{-4} Ω cm) in comparison with other TCOs. However, CdO is not very popular due to its small optical band gap (2.2 eV) and relatively poor optical transmittance in the short wavelength range (500-700 nm) [7]. The optoelectronic properties of CdO films can be tuned through doping with different transition and rare earth metal ions like Al, In, Ga, Mo, Ti, Sn, Eu, and Sm [7 - 14]. It was observed that when radius of dopant ions is smaller (or) more or equal than that of Cd^{2+}, then the optoelectronic properties of CdO thin films are improved [13]. Specifically 4f-metallic ions (rare earth metal ions) with smaller radius than that of Cd^{2+} are suitable for this purpose [15]. Literature survey shows that the rare earth metal ions are potential doping candidates for CdO thin films to tune the optical and electrical properties [15-17]. In this context, Dakhel [15] reported the improvement of electrical properties and deterioration of optical properties of Ce doped CdO thin films deposited by vacuum evaporation method. Pan et al. [16] reported that the Ce- and Gd- doped CdO films deposited by RF sputtering acquire low resistivity and high optical bang gap. Generally, Ce ions can exist in two different valence states: Ce^{3+} and Ce^{4+}, wherein Ce^{4+} ions may substitute some of Cd^{2+} ions in CdO crystalline structure. The 6-coordination ionic radius of Ce^{3+} and Ce^{4+} is 0.103 nm and 0.087 nm, respectively; among which, Ce^{4+} has small ionic radius in comparison with that of Cd^{2+} ion (0.097 nm) [18].

Including spray pyrolysis [10], CdO thin films were deposited by various techniques such as pulsed filtered cathodic arc

[1]Crystal Growth and Thin Films Laboratory, Department of Physics, Bharathidasan University, Tiruchirappalli- 620 024, Tamil Nadu, INDIA.
*Email : rampap2k@yahoo.co.in (Dr. R. Ramesh Babu)

[2]Crystal Growth and Thin Films Laboratory, Department of Physics and Nanotechnology, Faculty of Engineering and Technology, SRM University, Kattankulathur – 603 203, Tamil Nadu, INDIA.

[3]Nano-Optics and Optoelectronic (NOOR) Laboratory, iMicro, EECS Department, Masdar Institute, 54224 Abu Dhabi, UNITED ARAB EMIRATES.

deposition [8], vacuum evaporation [13, 15], and RF-magnetron sputtering [11, 19]. Hitherto, to the best of our knowledge, there is no report on the deposition and characterization of Ce-doped CdO films by spray pyrolysis technique. Hence in the present work, the influence of various low level of Ce-doping concentration on the structural, optical, morphological and electrical properties of CdO thin films prepared using a simple homemade chemical spray pyrolysis technique is reported.

Experimental details

CdO thin films were deposited on micro-slide glass substrates (Make: Labtech microscopic, soda lime glass slide) by spray pyrolysis unit [20]. Spray pyrolysis is a simple and suitable technique for large area deposition of almost any binary and ternary TCOs. The growth can easily be controlled by optimizing the deposition parameters such as spray rate, substrate temperature, dopant concentration, nozzle-substrate distance, nozzle frequency and carrier gas flow-rate. Reagent-grade cadmium acetate dihydrate ($Cd(CH_3COO)_2 \cdot 2H_2O$) (Merck, ≥98% purity) was used as the precursor for Cd. An appropriate quantity of cadmium acetate dihydrate was used to make 0.05 M solution by dissolving it in the mixed solvent of deionized water and methanol with 1:1 ratio. Different quantity of cerium chloride heptahydrate ($CeCl_3 \cdot 7H_2O$) (Sigma Aldrich, 99.9% purity) was added into the 0.05 M solution to deposit Ce- doped CdO films. The weight percentage of $CeCl_3 \cdot 6H_2O$ in solution was changed from 0.0 wt. % to 1.0 wt. % (0.25, 0.50, 0.75 and 1.0 wt. %). The glass substrates were ultrasonically cleaned prior to the deposition. The substrates were kept at 300 °C. The compressed and filtered air with a pressure of 45 kg / cm^2 was used as carrier gas. The distance between spray nozzle and the substrate was 30 cm. The deposition process was a two-step approach, which is consisting of a 1 s spray and 29 s dwell time. Except the Ce-doping concentration, all the other deposition conditions/parameters were kept constant during the experiments. The mixed solution was sprayed onto the preheated glass substrates. The high resistive chromel–alumel thermocouple was used to maintain the substrate temperature employing a digital temperature controller (INDFUR PID) (an accuracy of ± 5 °C). Fine droplets of the precursor solution were sprayed onto the substrates kept at 300 °C growth temperature. On process completion, the deposited films were allowed to naturally cool down to room temperature (RT). For each concentration, several sets of films were made and their structural, optical and electrical qualities were found to be reproducible.

Phase analysis was performed on the spray deposited undoped and Ce doped CdO thin films by means of X-ray diffraction (XRD) studies (PANalytical Empyrean X-ray diffractometer). All the films were characterized in Bragg-Brentano geometry, where θ and 2θ are coupled. The $CuK_{\alpha 1}$ wavelength (1.5406 Å) was used as X-ray source. The scan length for the diffraction angle (2θ) is ranging from 30° and 110° irrespective of the variation in the Ce- doping concentration. The thickness of CdO films was measured by Filmetrics (Model: F20-XT) and thickness of the films is around 300 nm ± 20 nm. Oxidation state analysis of the spray deposited Ce doped CdO films was carried out by X-ray Photo-electron Spectroscopy (XPS). Surface roughness and microstructure of the films were analyzed by atomic force microscopy (AFM) and FE-SEM (NovaNano from FEI). Elemental composition of thin films was analysed by energy dispersive X-ray spectroscopy (EDS) and inductive coupled plasma mass spectroscopy (ICP-MS) technique. The emission characteristics of Ce- doped CdO thin films were studied by photoluminescence (PL) spectral analysis. The van der Pauw technique (Ecopia – HMS 3000) was employed to estimate the resistivity, carrier mobility, carrier type, and carrier concentration at RT. The optical transmittance was recorded using Perkin Elmer make (Model: Lambda-35) spectrophotometer in the wavelength ranging from 200 nm to 1100 nm.

Results and discussion

Structural properties

The XRD patterns of undoped and Ce- doped CdO thin films are shown in Fig. 1. The existence of multiple diffraction peaks from (111), (200), (220), (311), (222), (400), (331), (420), and (422) planes confirm the polycrystalline nature of CdO thin films. The relatively stronger intensity of the peak obtained for undoped CdO thin film at $2\theta = 33.05°$ indicates the preferential growth along (111) orientation. All the diffraction peaks were indexed by matching with the standard data from international center for diffraction data (ICDD), reference code: 00-005-0640. Further, it is confirmed that the deposited films belong to cubic system and Fm-3m space group [21]. The lattice constant (*a*), texture coefficient (*TC*), crystalline size (*D*), dislocation density (δ), and microstrain (ε) were calculated from the XRD data and are presented in Table 1. The calculated *a* value is in good agreement with the reported value (4.695 Å) [21] (Table 1). For the initial Ce- doping (0.25 wt. %) in the precursor solution, the preferred orientation is shifted from (111) to (200) plane. The XRD intensity of (200) plane decreases with the further increase in Ce concentration (0.50 wt. %). At higher doping concentrations (0.75 and 1.0 wt. %), the preferred growth orientation is reverted back to (111) plane. This shift may be due to the substitution of Cd^{2+} (ionic radius - 0.097 nm) by Ce^{3+} or Ce^{4+} (ionic radius – 0.103 and 0.087 nm respectively) ions in the CdO lattice and thereby randomly altering the nucleation and growth processes of the deposited CdO thin films [14]**.** The increased peak intensity as well as the number of diffraction peaks with doping concentration is attributed to the improvement of crystallinity of Ce- doped CdO thin films. The preferred growth orientation along (111) plane for undoped CdO thin film and that of In, Al, and Ga doped CdO films are already reported [7-9]. The *TC* of CdO thin films is estimated using the following relation [22]

$$TC = \frac{\left[\frac{I_m(hkl)}{I_o(hkl)}\right]}{\left[\frac{1}{N}\Sigma\frac{I_m(hkl)}{I_o(hkl)}\right]} \quad (1)$$

where $I_{m(hkl)}$ is the measured relative intensity of reflections from a given (hkl) plane, $I_{o(hkl)}$ is the relative intensity of reflections from the same plane as indicated in a standard sample of randomly oriented polycrystalline CdO powder [21] and N is total number of reflections observed, which is 9 in the present case. The deviation of *TC* of a particular plane from unity implies the preferred orientation along that plane. The calculated *TC* values are given in Table 1, which clearly indicate the decrease of *TC* value for (111) plane, from 2.6256 to 1.5764. At the same time, *TC* value for (200) plane is increased from 1.8656 to 2.8061 with respect of Ce concentration. The mean X-ray crystallite size of (200) plane was estimated using Scherrer's formula [23]

$$D = \frac{0.9\,\lambda}{\beta \cos\theta} \qquad (2)$$

where 'β' is the full-width half maximum (FWHM) of the corresponding diffraction peak and 'λ' is the X-ray wavelength (1.5406 Å). The results are given in Table 1, which show that for higher doping concentration (1.0 wt. %) the crystallite size is increased when compared to that of pure CdO and is decreased when compared to that of CdO doped with 0.75 wt. %. It is found that the size of crystallites varies from 21 nm to 27 nm with respect to systematic increase in the Ce- doping concentration up to 0.75 wt.%. The micro-strain and dislocation density was calculated using the relation [24],

$$\varepsilon = \frac{\beta \cos\theta}{4} \quad \text{and} \qquad (3)$$

$$\delta = \frac{1}{D^2} \qquad (4)$$

and the calculated values are given in Table 1. The average strain and dislocation density values initially decrease then increase with increasing Ce- doping concentration. The small value of *'δ'* obtained for 0.50 wt. % of Ce in the present work confirms that spray pyrolysis is an effective technique to deposit good quality polycrystalline CdO thin films. The micro-strain values decrease with respect to doping concentration of Ce in CdO thin films up to 0.50 wt. %. This type of micro-strain changes can be related to the crystallization process in polycrystalline thin films and also ionic radius of impurity ions since the ionic radius of Ce^{3+} or Ce^{4+} ion is slightly smaller or more than that of Cd^{2+} ions. Hence, it will induce the strain in CdO lattices and alter the nucleation processes and change the crystalline quality. XRD studies showed that 0.5 wt. % of Ce-doped CdO thin films have good crystallinity, low strain and less dislocation density when compared with that of the CdO and Ce- doped CdO films deposited in this work.

XPS analysis

XPS analysis was carried out on 1.0 wt. % Ce- doped CdO thin films in order to figure out the oxidation states of Ce, Cd, and O elements. The different spectra obtained using MgKα radiations at 1.2536 keV are comparatively shown in Fig. 2. A wide survey scan of XPS spectrum is shown in Fig. 2a. The binding energy corresponding to the peaks Cd $3d_{5/2}$,Cd $3d_{3/2}$, Cd $3p_{3/2}$, Cd $3p_{1/2}$, Ce $3d_{5/2}$ and O1s as obtained from XPS analysis are 406 eV (405.07 eV), 413 eV (411 eV), 618 eV (617.06 eV), 652 eV (650.57 eV), 878-882 eV (882.70 eV), and 530 (532 eV) eV respectively. These values are in good agreement with the reported values given in parenthesis [25, 26]. The narrow scan spectrum of Cd, O and Ce elements are shown in Figs. 2b-d. The Cd 3d features the main Cd $3d_{5/2}$ and Cd $3d_{3/2}$ spin orbit components. The binding energy of Cd $3d_{5/2}$ (Fig. 2b) indicates the Cd^{2+} states; this is in good agreement with the literature [25]. The binding energy corresponding to the peak O1s obtained from XPS analysis is 530 eV which confirms the presence of O^{2-} oxidation state in the deposited film (Fig. 2c). A less intense binding energy peak at 878 and 882 eV may be attributed to the Ce $3d_{5/2}$ with Ce^{3+} and Ce^{4+}oxidization states, respectively [26].

Surface microstructural properties

Surface microstructures and roughness of undoped and Ce-doped thin films were analyzed by AFM because these two are very critical in optoelectronic device applications. The roughness not only describes the light scattering phenomena but also gives more information on the quality of the surface under investigation [27]. Two dimensional (2D) and three dimensional (3D) surface microstructures of CdO and Ce doped CdO thin films with different Ce- doping concentration are shown in Figs. 3(a-e) and Fig.3(a_1-e_1) respectively (scan area: 0.5 µm × 0.5 µm). A careful study on the microstructures reveals that undoped CdO thin films (Fig. 3a, a_1) are comprised of spherical shaped grains along with the agglomerated spheroidal shaped grains, which are uniformly distributed on the substrate surface. As the level of Ce- doping is increased to 0.25 wt. %, the film surface becomes more uniform and smooth (Fig. 3b, b_1) in comparison with that of the undoped films. Further increase in Ce- doping concentration (0.50 wt. %, 0.75 wt. % and 1.0 wt. %) also leads to some agglomeration and porous structures (Figs. 3c-e, c_1-e_1) with smaller grains. This may be due to the fact that randomly distributed nuclei formed initial growth into observable grains, because the crystallization process involves various stages of nucleation, growth and coalescence during the deposition of thin film. These steps are also observed in La- doped ZnO thin films [28]. The root mean square (RMS) roughness values are varied with the variation in cerium chloride concentrations in the precursor solution as follows: 2.24 nm, 2.88 nm, 2.96 nm, 2.86 nm, and 1.22 nm for undoped, 0.25 wt. %, 0.5 wt. %, 0.75 wt. %, and 1.0 wt. % CdO: Ce films, respectively (Table 2). AFM analysis showed that the 0.5 wt. % Ce doped CdO thin films are slightly rougher than undoped and other Ce- doped CdO thin films. Increase in the surface roughness with increasing Ce concentrations is associated with the increase in grain size of the films. It can be concluded that the average surface roughness of the CdO thin films is thus modified by Ce concentration in the films.

The surface microstructures of CdO thin films obtained from FE-SEM analysis are compared in Fig. 4 as a function of Ce

concentration. Figure 4a shows the surface microstructure of undoped CdO thin film, which consists of uniformly distributed spherical shaped grains together with some small patches and agglomerations. Figs. 4b-e show the surface microstructures obtained from the films deposited from 0.25 wt. %, 0.50 wt. %, 0.75 wt. %, and 1.0 wt. % of cerium chloride concentration in the solution, respectively. Improved grain size and enhanced surface uniformity were observed in the films doped with 0.25 wt. % Ce and 0.50 wt. % Ce (Figs. 4b and 4c, respectively). The surface microstructure shown in Fig. 4d reveals uniform distribution of grains with more regular shapes, and decreased size. The surface of the film doped with 1.0 wt. % of Ce (Fig. 4e) consists relatively small sized grains and elongated spherical shaped grains and the surface microstructures show small voids and pinholes. The average grain size (*d*) of the undoped and Ce- doped CdO films is measured from the corresponding FE-SEM microstructures and are plotted as histogram images in Figs. 5a-e. The average grain size of undoped CdO film is increased from 64 nm to 98 nm and to 134 nm, following the increase in Ce doping to 0.25 wt. % and 0.50 wt. %, respectively. However, further increase in Ce-doping concentration decreases the average grain size from 134 nm (0.50 wt. %) as follows: 113 nm for 0.75 wt. % and 87 nm for 1.00 wt. % Ce doping (Table 2). The grain size calculated from FE-SEM is greater when compared with the grain size calculated from XRD, because symmetrical reflection like XRD determines the coherence length due to lattice atoms of crystalline materials whereas the surface probes like FE-SEM estimates the agglomerated structures on the surface of the film [11]. The foregoing discussion clearly indicates that the surface microstructures of CdO thin film are effectively modified by Ce- doping concentration and 0.50 wt. % Ce-doped CdO thin film has uniformly distributed grains in comparison with the undoped and other Ce doped CdO thin films. Typical EDS spectrum obtained from 0.5 wt. % Ce- doped CdO film (Fig. 6) shows the presence of Cd (L_α spectral lines),O (K_α spectral lines) and Ce (L_α spectral lines) along with some signals from glass substrate. The ratio of intensity of Cd, O and Ce are determined by relative weight and atomic ratios of Cd, O and Ce. The measured ratios are given in Table 2, which clearly indicates the presence of Ce in the spray deposited CdO thin films. Furthermore, the films were subjected to ICP-MS analysis and obtained values are given in Table 2, which shows that level of Ce dopants present in the CdO thin films.

Electrical properties

Hall measurements confirm that the films are highly conducting. The variation in electrical properties such as carrier concentration (n_e), carrier mobility (μ_e), resistivity (ρ) and conductivity (σ) of CdO thin films are shown in Figs. 7 and 8 as a function of Ce concentration. The negative sign of Hall coefficient confirms n- type conductivity. The carrier concentration of CdO thin films is increased with increasing Ce concentration up to 0.5 wt. %, and then decreased for higher doping concentrations. It may be attributed that when the Ce doping concentration is above 0.50 wt. %, Ce^{3+} acts as neutral impurity and increasing the neutral impurity scattering (NIS) which limit the carrier concentration and also mobility and hence the change in the surface morphology [29]. A high carrier concentration of 3.85×10^{20} cm^{-3} is obtained for 0.50 wt. % Ce- doped CdO thin films. The measured values are given in Table 3. A low resistivity (3.81×10^{-4} Ω cm) and high conductivity (2.62×10^{3} Ω^{-1} cm^{-1}) are observed for 0.5 wt. % Ce- doped CdO thin films (Fig. 8). The increasing carrier concentration may be attributed to the substitution of Ce^{3+} for Cd^{2+} in the CdO lattice, which results in more free electrons that contribute to the electrical conductivity. In the present work, we can observe that slight Ce- doping improves the conduction parameter (carrier concentration, conductivity and resistivity) of CdO thin films so that the 0.50 wt. % Ce- doped CdO films shows an increase in carrier concentration about 3.8 times, conductivity about 2.5 times; and decreases the resistivity about 2.5 times, in relation with the undoped CdO thin films.

Optical properties

The optical transmittance spectra of spray deposited undoped and Ce- doped CdO thin films as a function of Ce- doping concentration are given in Fig. 9. It is observed that all the deposited Ce- doped CdO films exhibited high transmittance of about 80 % in the wavelength range of 600 – 1100 nm and optical transmittance of the films is increased with increase in Ce concentration. The observed blue shift of absorption edge is due to the Ce doping (Fig. 9). The average transmittance (AT - 600 -1100 nm) of CdO increases from 72 % to 86 % for the initial Ce doping concentration (0.25 wt. %) and AT remains nearly the same for other Ce concentration (84 % for 0.50 wt. %, 85 % for 0.75 wt. % and 84 % for 1.0 wt. %). The blue shift of absorption edge is called band gap widening (BGW), which can be explained by the Moss–Burstein (M–B) effect [30]. Burstein pointed out that the lifting of the Fermi level up to the conduction band might cause the band gap broadening in degenerated semiconductor. The absorption coefficient (α) as a function of wavelength (λ) is calculated using the following relation [31]

$$\alpha(\lambda) = \frac{1}{t} \ln\left(\frac{1}{T}\right) \quad (5)$$

Where *T* is the transmittance and *t* is the thickness of the films. The relation between the α and the incident photon energy ($h\nu$) is given by the following equation [31]

$$(\alpha h\nu) = A(h\nu - E_g)^m \quad (6)$$

Where *'A'* is energy independent constant, E_g is optical band gap and *'m'* is an index, which depends on the kind of optical transition. Specifically, *m* is 1/2, 3/2, 2 and 3 when the transition is direct-allowed, direct-forbidden, indirect-allowed, and indirect-forbidden, respectively. From the theoretical and experimental results, CdO film is known to be a direct-allowed semiconducting material [15, 16]. The direct optical band gap was calculated from $(\alpha h\nu)^2$ *vs* $h\nu$ plot by extrapolating the linear portion to $h\nu$ axis (Fig. 10). Extrapolating the linear

portion of the plot onto the energy axis gives the band gap value of the film, which is gradually increased from 2.38 to 2.63 eV with increase in Ce concentration from 0.25 to 1.0 wt. %. The obtained values are summarized in Table 3. Thus, the present results reveal that Ce- doping increases the transmittance (600-1100 nm) and the band gap value of CdO film. Present values with the corresponding reported values by Dakhel [15], are compared in Table 3 which shows that the present values are relatively improved.

Photoluminescence studies

Figure 11 illustrates the PL spectra of the CdO and Ce- doped CdO thin films recorded at RT. All the samples are excited at the wavelength of 325 nm. The PL spectra of the undoped and Ce- doped CdO thin films exhibit various emission features, and doping concentration changes the intensity and the position of PL emission peak. Two sharp peaks and one less intense broad peak are present in these spectra. The peak located at 418 nm may be due to an exciton bound to a donor level [32]. The high intense PL peak obtained at 522 nm (green emission) for CdO film may be due to deep-level or trap-state emission, corresponding to the ionized oxygen vacancies in the CdO thin films [33]. For higher doping concentration, intensity of the peak is increased and peaks are slightly shifted towards lower energy (522 nm - 539 nm). The broad band observed (650 – 750 nm) in the photoluminescence spectrum of CdO thin film indicates the defect-related luminescence peak. This may be due to the radiative transitions between oxygen vacancies or Cd interstitials acting as shallow donors and Cd vacancies acting as deep acceptors [34].

Opto-electronic properties – Figure of merit

The figure of merit (FOM) plays an important role in optoelectronic device applications. In this work, to analyse the effect on the combination of optoelectronic performance of Ce doped CdO thin films, the FOM values were calculated. The calculations were made using the formula proposed by Tvarozek et al. [35]

$$FOM = \frac{T^{opt}}{R_{sh}} \quad (7)$$

Where T^{opt} is the optical transmittance for average wavelength (600-1100 nm) and the formula proposed by Haacke [36] for transparent conducting oxide thin films

$$FOM = \frac{T^{10}}{R_{Sh}} \quad (8)$$

where T^{10} is transmittance at a particular wavelength and R_{sh} is sheet resistance of CdO and Ce doped CdO thin films. Figure of merit values calculated for different wavelengths are given in Table 4. Tvarozek et al. [35] showed that the materials possessing figure of merit above 1.0 % Ω^{-1} provide better performance and are suitable for TCO application. In the present work, all the spray deposited films have (FOM > 1.0 %) high FOM, the value varied from 1.93 % to 4.40 % / Ω. Among the various Ce doping concentration 0.5 wt. % has 4.40 % /Ω of FOM (Table 4). It can be also noticed that the 0.5 wt. % of Ce doped CdO thin film has a high figure of merit (9.18×10^{-3} % Ω^{-1}) (Fig. 12). Thus the results show that the film doped with 0.50 wt. % Ce has a high optical transmittance, high electrical conductivity, low resistivity and high figure of merit.

Conclusions

Various levels of Ce doping modified the structural, optical and electrical properties of CdO thin films. XRD studies confirmed the single phase CdO with cubic structure and polycrystalline quality and the shift in preferred growth orientation from (111) plane to (200) plane for 0.25 wt. % Ce-doping, which is validated by *TC* values. The grain size of CdO thin films slightly varies between 21 nm and 27 nm due to the various level of Ce- doping. AFM analysis confirmed the modification of the surface microstructures of CdO thin films due to Ce- doping. RMS roughness value varies from 1.22 nm to 2.96 nm. High carrier concentration (3.85×10^{20} cm^{-3}) and low resistivity (3.81×10^{-4} Ω cm) is observed for 0.50 wt. % of Ce doped CdO thin films. Transmittance spectrum shows that the transmittance of deposited CdO thin film is increased with the increasing Ce- concentrations. The AT and band gap are in the range of 72 % - 86 %, and 2.38 eV - 2.63 eV, respectively. Ce doping of 0.5 wt. % is reduced the sheet resistance nearly half of the CdO film. The PL measurements showed that the CdO and Ce- doped CdO films have strong luminescence behavior. High figure of merit value is obtained for 0.50 wt. % of Ce- doped CdO thin films. The low sheet resistance, high conductivity and improved optical properties are achieved in the spray deposited Ce doped CdO thin films. Thus the results obtained in the present work indicate that the deposited films from a simple homemade and cost effective spray pyrolysis technique could be useful in the field of TCO.

Acknowledgements

The author, P. Velusamy sincerely acknowledge the Bharathidasan University, Tiruchirappalli-620 024 for the financial support provided to carry out this work under the University Research Fellowship Scheme (URF - Ref. No. 47363/Ph.D1/2010). The author E. Elangovan thanks Mike Tiner, Mustapha Jouiad, and Leslie George from Masdar Institute for XRD, FE-SEM and cleanroom facilities, respectively.

References

1 A. Stadler, *Materials*, 2012, **5,** 661-683.
2 K. Fleischer, E. Arca, I.V. Shvets, *Sol. Energy Mater. Sol. Cells,* 2012, **101**, 262–269.
3 R. Chandiramouli, B.G. Jeyaprakash, *Solid State Sciences,* 2013, **16** 102-110.
4 M.K. Al Turkestani, K. Durose, *Sol. Energy Mater. Sol. Cells,* 2011, **95**, 491–496.

5 S. Girish Kumar and K. S. R. Koteswara Rao, *Energy Environ. Sci.* 2014, **7,** 45-102.
6 A. Dakhel, J Mater Sci, 2011, **46,** 6925-6931.
7 R. Kumaravel, S. Menaka, S. Regina Mary Snega, K. Ramamurthi, K. Jeganathan, *Mater. Chem. Phys.*, 2010 **122,** 444-448.
8 Y. Zhu, R. J. Mendelsberg, J. Zhu, J. Hana Andre Anders, *Appl. Surf. Sci*. 2013, **265,** 738– 744.
9 A.V. Moholkar, G. L. Agawane, K. Ung Sim, Y. Kwon, D. Sun Choi, K. Y. Rajpure, J. H. Kim, *J. Alloys Compd.,* 2010 **506,** 794–799.
10 R. Kumaravel, S. Bhuvaneswari, K. Ramamurthi, V. Krishnakumar, Appl Phys A Material Science & Processing, 2012, **109,** 579–584.
11 B. Saha, R. Thapa, K.K. Chattopadhyay, Solid State Communications, 2008, **145**, 33–37.
12 B. J. Zheng, J.S. Lian, L. Zhao, Q. Jiang, *Vacuum,* 2011, **85,** 861-865.
13 A. A. Dakhel, Opt. Mater, 2009, **31**, 691–695.
14 P. Velusamy, R. Ramesh Babu, K. Ramamurthi, J. Viegas, E. Elangovan, J Mater Sci: Mater Electron, 2015, **26,** 4152–4164.
15 A. A. Dakhel, *Mater. Chem. Phys*, 2011, **130,** 398– 402.
16 L. L. Pan, G. Y. Li, J. S. Lian, *Appl. Surf. Sci*, 2013, **274,** 365–370.
17 P. Chen, Z. He, H.Y. He, Journal of Ceramic Processing Research, 2013, **14,** 56-58.
18 Kenneth Barbalace. Periodic Table of Elements - Sorted by Ionic Radius. EnvironmentalChemistry.com. 1995 - 2015. Accessed on-line: 11/16/2015 http://EnvironmentalChemistry.com/yogi/periodic/ionicradius.html.
19 B. Saha, R. Thapa, K. K. Chattopadhyay, *Sol. Energy Mater. Sol. Cells,* 2008, **92,** 1077–1080.
20 T. Indira Gandhi, R. Ramesh Babu, K. Ramamurthi, *Mater. Sci. Semicond. Process,* 2013, **16,** 472-479.
21 Powder Diffraction File, *International Centre for Diffraction Data (ICDD)*, Reference Code: 00-005-0640.
22 A.H. K. Elttayef, H. M. Ajeel, A. I. Khudiar, *J Mater Res Technol*. 2013, **2,** 182–187.
23 A.A. Dakhel, *J. Alloys Compd*, 2009, **475,** 51–54.
24 M. Azizar Rahman, M.K.R. Khan, Materials Science in Semiconductor Processing 2014, **24,** 26–33.
25 L. L. Pan, K. K. Meng, G. Y. Li, H. M. Sun and J. S. Lian, *RSC Adv.,* 2014, **4**, 52451-524560.
26 C. Zhang, J. Lin, *Phys. Chem. Chem. Phys*., 2011, **13,** 3896–3905.
27 A. Abdolahzadeh Ziabari, F.E. Ghodsi, G.Kiriakidis, *Surf. Coat. Technol*., 2012, **213,** 15-20.
28 Y. Bouznit, Y. Beggah, F. Ynineb, *Appl. Surf. Sci,* 2012, **258,** 2967-2971.
29 D. S. Ginley, D. C. Paine, H. Hosono, Handbook of Transparent Conductors, Springer, New York, 2010, 265-293.
30 E. Burstein, *Phys. Rev*. 1954, **93,** 632-633.
31 I. S. Yahia, G. F. Salem, M. S. Abd El-sadek , F. Yakuphanoglu, Superlattice. Microst., 2013, **64**, 178–184.
32 Z. R. Khan1, M. S. Khan, M. Zulfequar, M. Shahid Khan, *Materials Sciences and Applications*, 2011, **2,** 340-345.
33 F.E. Ghodsi, H. Absalan, *Acta Phys. Pol., A ,* 2010, **118,** 659-663.
34 Z. Pan, P. Zhang, X. Tian, G. Cheng, Y. Xie, H. Zhang, X. Zeng, C. Xiao, G. Hu, Z. Wei, J. Alloys Compnds. 2013, **576**, 31-37.
35 V. Tvarozek, P. Sutta, S. Flickyngerova, I. Novotny, P. Gaspierik, M. Netrvalova, E. Vavrinsky (2010). Preparation of Transparent Conductive AZO Thin Films for Solar Cells, Semiconductor Technologies, Jan Grym (Ed.), ISBN: 978-953-307-080-3.
36 G. Haacke, *J. Appl. Phys*. 1976, **47,** 4086-4089.

Table 1. Lattice constant (*a*), crystallite size (*D*), dislocation density (δ), micro strain (ε) and texture coefficient (*TC*) of undoped and Ce- doped CdO thin films.

Plane	Doping concentration (Ce) (wt. %)	(a) (Å)	(D) (nm)	(δ) (10^{15} Line /m^2)	(ε) ($x10^{-3}$)	TC value	
						(200)	(111)
(200)	0.00	4.6912	21	2.331	1.68	1.8656	2.6256
	0.25	4.6916	23	1.820	1.48	2.8061	1.5764
	0.50	4.6934	26	1.394	1.29	2.7314	1.5806
	0.75	4.6936	27	1.512	1.35	2.2510	1.9950
	1.00	4.6942	23	1.862	1.50	1.8319	2.2429

Table. 2 Roughness, average grain size (d) from FE-SEM analysis and Elemental compositions of CdO films obtained from EDS

Ce doping Concentration (wt. %)	'd' (nm) (FE-SEM)	Roughness (nm) (AFM)	Percentage of Elements (wt. %)			Percentage of Elements (at. %)			ICP-MS (ppb)	
			O (K series)	Cd (L series)	Ce (L series)	O (K series)	Cd (L series)	Ce (L series)	Cd	Ce
0.00	64	2.24	14.29	85.71	0.00	53.94	46.06	0.00	---	---
0.25	98	2.88	15.63	84.19	0.18	56.20	43.65	0.16	---	---
0.50	134	2.96	20.07	79.01	0.40	58.00	41.80	0.20	19.18	0.73
0.75	113	2.86	16.41	83.10	0.49	52.63	46.82	0.56	15.20	0.84
1.00	87	1.22	14.12	85.12	0.76	63.14	36.22	0.64	16.50	1.25

Table 3. Comparison of electrical and optical properties of Ce doped CdO thin films prepared by different preparation techniques.

Doping % (Ce) (wt. %)	n_e (10^{20} / cm^3)	μ_e (cm^2 / V.s)	ρ (10^{-4} Ω m)	σ (10^3/Ω cm)	AT (%) (600 -1100 nm)	E_g (eV)	Deposition technique	Reference
0.00	1.01	69	9.32	1.07	72	2.38	Spray pyrolysis	Present work
0.25	2.74	42.4	5.36	1.86	86	2.52	Spray pyrolysis	Present work
0.50	3.85	40	3.81	2.62	84	2.54	Spray pyrolysis	Present work
0.75	3.35	32.47	5.72	1.74	85	2.61	Spray pyrolysis	Present work
1.00	3.24	27.86	6.9	1.44	84	2.63	Spray pyrolysis	Present work
3.8 at.% Ce	2.42	66.71	3.86	---	60	2.08	Vacuum evaporation	[15]

Table 4. Figure of merit of undoped and Ce- doped CdO thin films with different wavelengths.

Doping % (Ce) (wt. %)	R_{Sh} (Ω / □)	Figure of Merit (FOM) (10^{-3} Ω^{-1}) [36]							FOM (% /Ω) (T^{opt}/R_{sh}) [35]
		600 nm	700 nm	800 nm	900 nm	1000 nm	1100 nm	AT (600-1100 nm)	
CdO	37.28	0.27	0.55	0.910	1.48	2.00	2.19	1.00	1.93
0.25	26.80	8.59	9.38	8.17	7.23	7.31	7.90	8.26	3.26
0.50	19.05	6.20	7.44	7.95	8.86	1.09	1.36	9.18	4.40
0.75	28.28	3.74	4.94	6.14	7.71	1.02	1.30	6.96	3.00
1.00	34.50	2.73	3.48	4.21	5.23	6.92	9.00	5.07	2.30

RSC Advances

ARTICLE

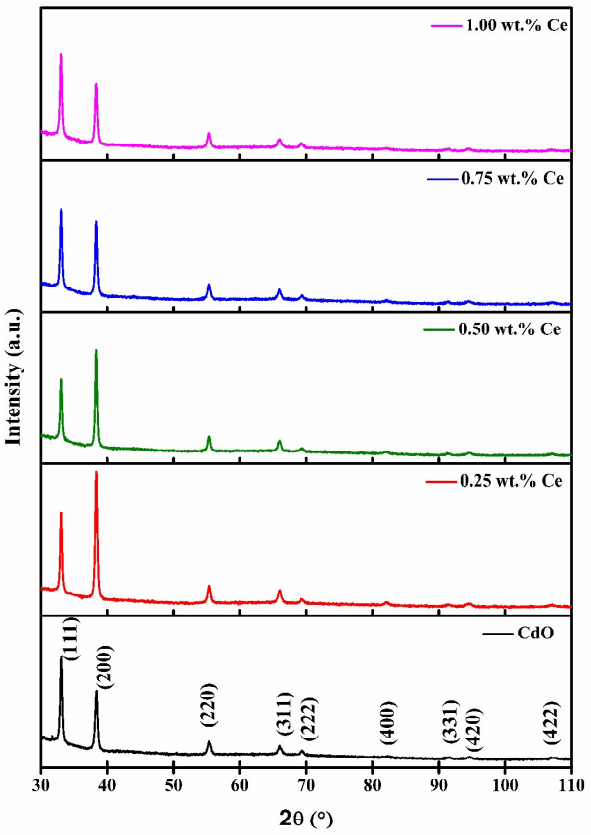

Figure 1 XRD patterns of CdO thin films as a function of Ce doping concentration.

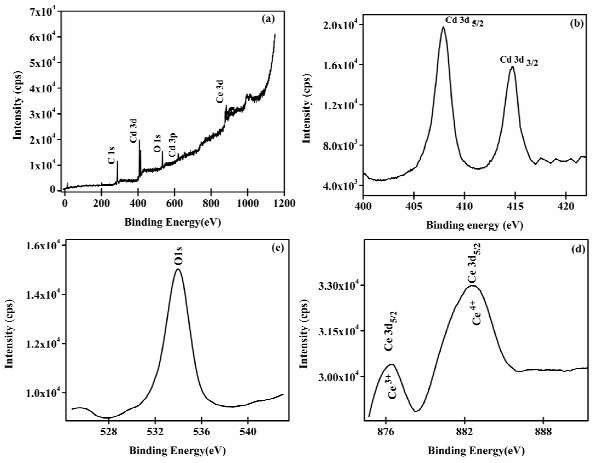

Figure 2 A typical XPS spectrum of 1.0 wt. % Ce doped CdO thin film.

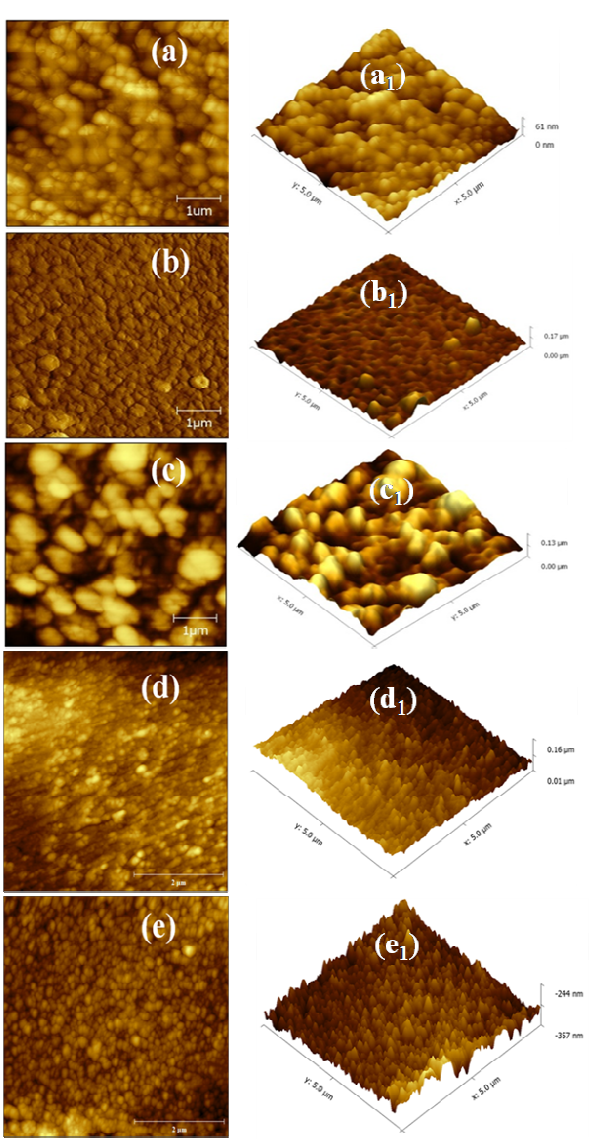

Figure 3 2D and 3D surface microstructures obtained from AFM analysis: (a,a_1) Undoped CdO (b, b_1) 0.25 wt. % Ce doped CdO, (c, c_1) 0.50 wt. % Ce doped CdO, (d, d_1) 0.75 wt. % Ce doped CdO, and (e, e_1) 1.0 wt. % Ce doped CdO.

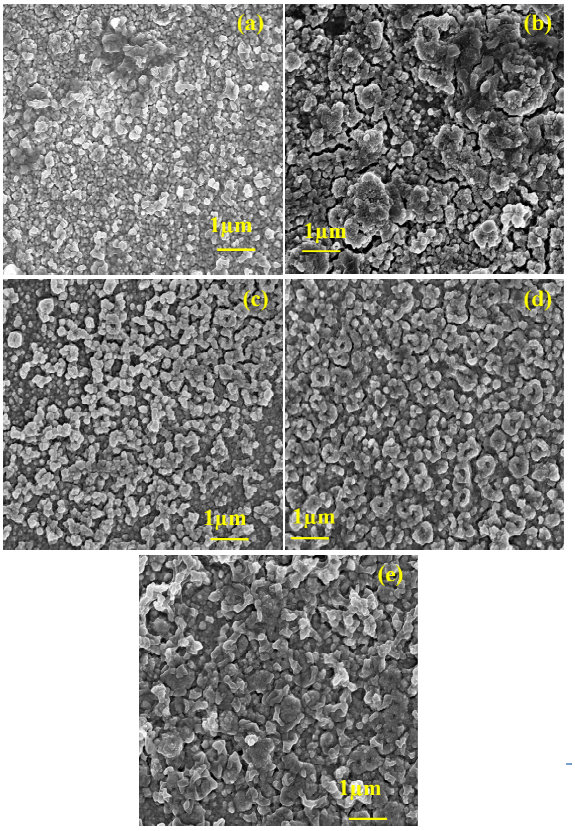

Figure 4 FE-SEM microstructures of CdO thin films obtained from FE-SEM analysis: (a) Undoped CdO (b) 0.25wt. % Ce doped CdO, (c) 0.50 wt. % Ce doped CdO, (d) 0.75 wt. % Ce doped CdO, and (e) 1.0 wt. % Ce doped CdO.

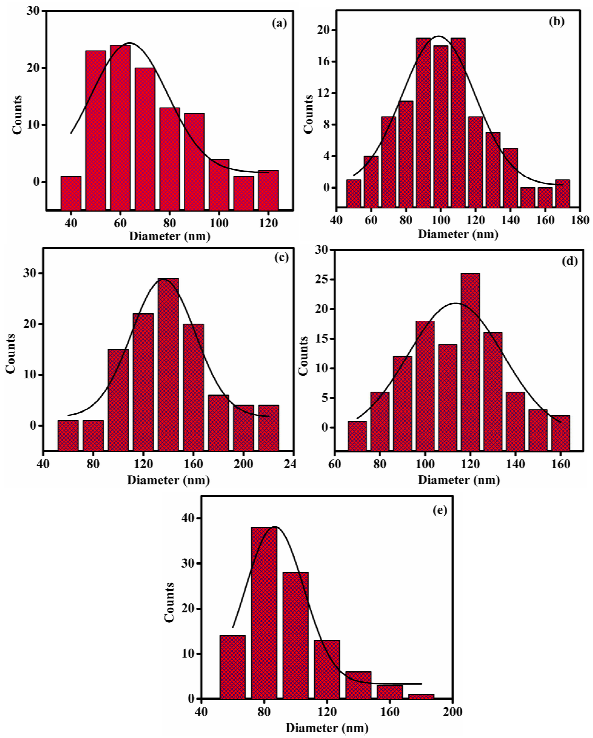

Figure 5 Average grain size obtained by Histogram image: (a) Undoped CdO (b) 0.25wt. % Ce doped CdO, (c) 0.50 wt. % Ce doped CdO, (d) 0.75 wt. % Ce doped CdO, and (e) 1.0 wt. % Ce doped CdO.

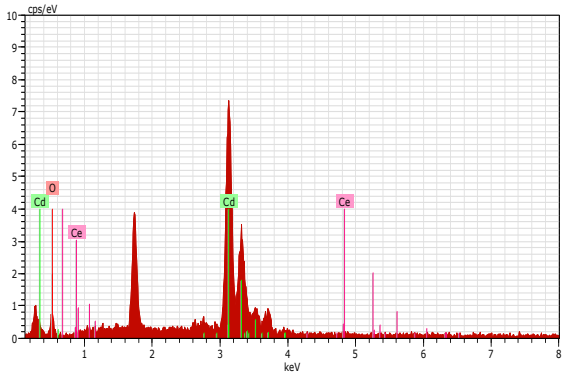

Figure 6 Typical EDX spectrum obtained from 0.50 wt. % Ce doped CdO thin films.

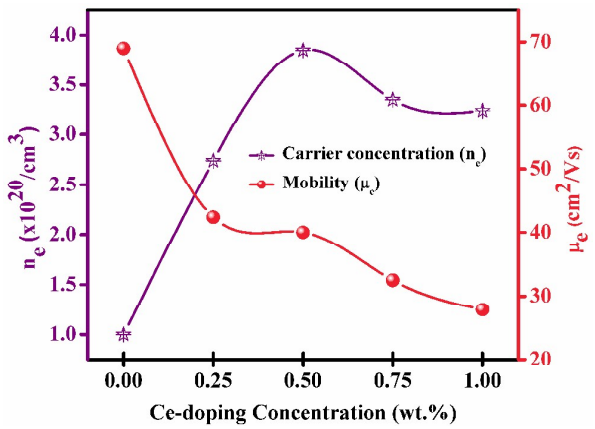

Figure 7 Variation in mobility and carrier concentration of CdO thin films as a function of Ce doping concentration.

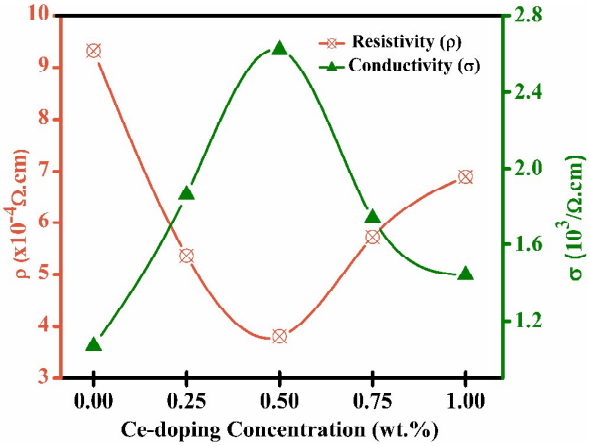

Figure 8 Variation in resistivity and conductivity of CdO thin films as a function of Ce doping concentration.

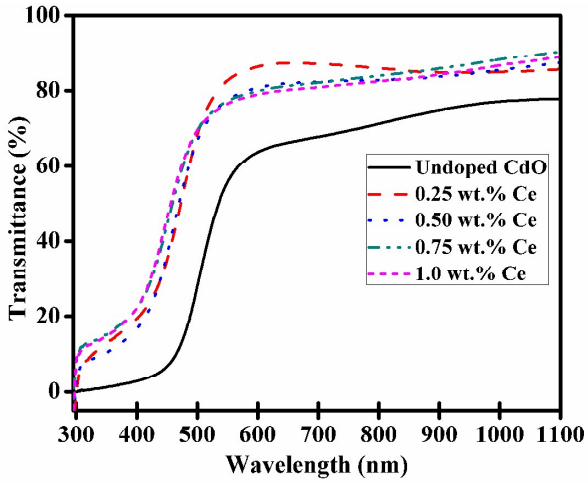

Figure 9 Optical transmittance spectra of CdO thin films as a function of Ce doping concentration

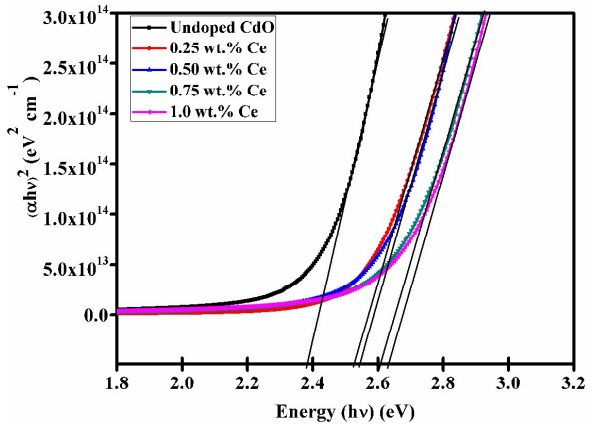

Figure 10 Plot of $(\alpha h\nu)^2$ *vs* photon energy ($h\nu$) to estimate the optical band gap of undoped and Ce doped CdO thin films.

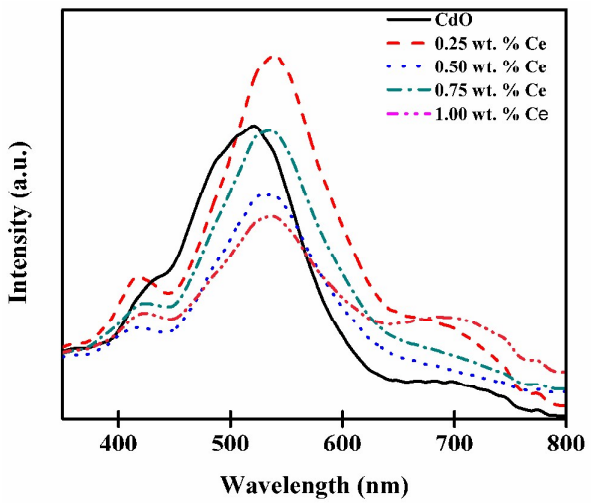

Figure 11 Photoluminescence spectrum of undoped and Ce doped CdO thin films.

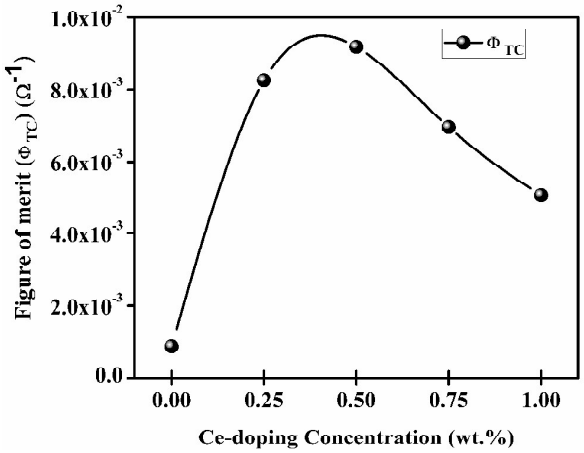

Figure 12 Figure of merit obtained from CdO as a function of Ce doping concentration.

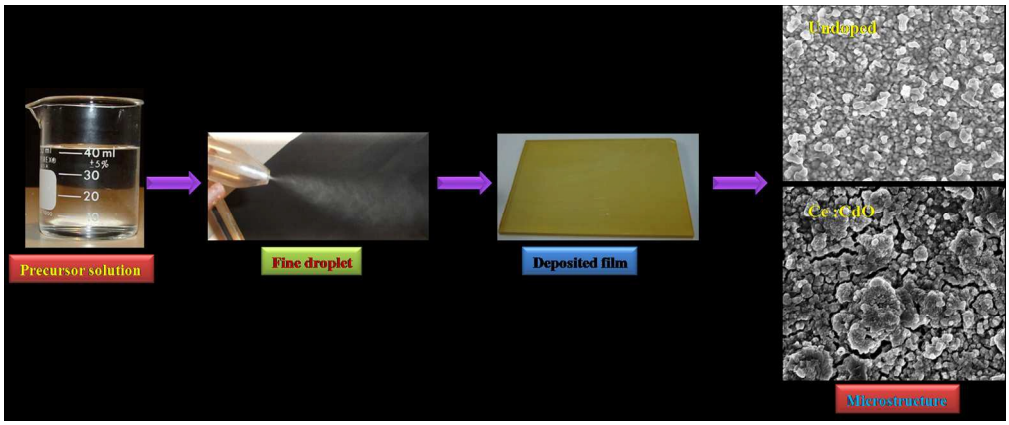

277x114mm (150 x 150 DPI)